Phonon emission by photoexcited carriers in InGaN/GaN multiple quantum wells

2002 J. Phys.: Condens. Matter 14 3445

(http://iopscience.iop.org/0953-8984/14/13/304)

INSTITUTE OF PHYSICS PUBLISHING JOURNAL OF PHYSICS: CONDENSED MATTER

J. Phys.: Condens. Matter **14** (2002) 3445–3455 PII: S0953-8984(02)26667-9

Phonon emission by photoexcited carriers in InGaN/GaN multiple quantum wells

A V Akimov[1], S A Cavill[1], A J Kent[1], N M Stanton[1], T Wang[2] and S Sakai[2]

[1] School of Physics and Astronomy, University of Nottingham, University Park, Nottingham NG7 2RD, UK
[2] Satellite Venture Business Laboratory, Department of Electrical and Electronic Engineering, The University of Tokushima, Minami-josanjima, Tokushima 770, Japan

Received 9 July 2001
Published 22 March 2002
Online at stacks.iop.org/JPhysCM/14/3445

Abstract

The effect of well width on both the photoluminescence (PL) and phonon emission in optically excited InGaN multiple quantum well (MQW) samples has been investigated. For narrow MQW samples ($w < 2.5$ nm), the low-temperature PL quantum efficiency is close to unity with the phonon emission being due mainly to carrier relaxation in the QWs. For wider MQWs samples the PL quantum efficiency is reduced and the intensity of the phonon emission increases. We explain this in terms of the non-radiative recombination processes in the QWs which result in phonon emission and compete with the radiative process.

1. Introduction

The optical properties of InGaN/GaN multiple quantum wells (MQWs) have been the subject of considerable interest recently. This has been driven by their applications in blue/green light emitting diodes [1] and blue laser diodes [2,3]. Studies of the optical properties of InGaN/GaN MQWs have been reported by many research groups, see for example [4–8] and references therein. Their work was aimed at understanding the radiative recombination mechanisms and their relationship to material characteristics. It has been demonstrated that high-quality InGaN/GaN MQWs exhibit strong photoluminescence (PL) at room temperatures and, at low temperatures, the quantum efficiency of PL is close to unity. In high-quality samples the minimum PL spectral linewidth measured is about 45 meV [4, 5].

Non-radiative processes are also central to the behaviour of MQW-based optoelectronic devices. These non-radiative processes include (see figure 1) the relaxation of hot quasiparticles (carriers and excitons) and also non-radiative recombination at defects, which competes with PL reducing the PL quantum efficiency. The relaxation of hot quasiparticles in MQWs should have specific features related to two-dimensional confinement effects. Thus this process may be very different from the relaxation of hot carriers in bulk GaN reported recently [9]. Normally,

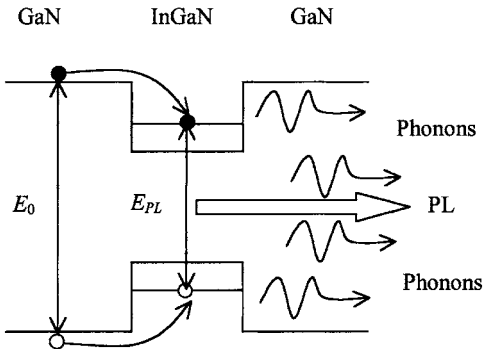

Figure 1. The scheme of radiative (PL) and non-radiative transitions in an InGaN/GaN QW.

information about the non-radiative processes is inferred indirectly from PL measurements. However, these processes also involve the emission of phonons which may be detected to give more detailed information.

The emission of phonons by hot quasiparticles is governed by the selection rules and the oscillator strength for carrier (exciton)–phonon transitions. Longitudinal optic (LO) phonon emission due to the Fröhlich interaction in a polar semiconductor is normally the dominant energy relaxation process. If the carrier excess energy is not enough for the emission of LO phonons, longitudinal (LA) and transverse (TA) acoustic phonons are emitted. The selection rules for electron–acoustic phonon interaction in QWs give that, in narrow QWs, acoustic phonons are emitted mostly perpendicular to the plane of the QW. This effect was demonstrated earlier in AlGaAs/GaAs QWs [10]. Acoustic phonon emission in GaN-based nanostructures has not yet been detected directly. There are several reasons which make the interaction of phonons with carriers and excitons different from GaAs-based structures: (i) the large LO phonon energy, 92 meV in GaN as compared to 36 meV in GaAs, (ii) strong piezoelectric (PE) constant of GaN, at least five times stronger than in GaAs, and (iii) the higher impurity and defect density in GaN-based MQWs.

The main aim of this work was to obtain information about non-radiative processes in InGaN/GaN MQWs from studies of the phonons emitted. There were two main objectives: (1) to understand the relaxation processes for hot optically excited quasiparticles and to find the experimental conditions where the carrier– and exciton–phonon interaction is governed by the two-dimensional nature of the carrier states in the QWs; and (2) to show that in high-quality InGaN/GaN narrow MQW structures the phonon emission comes mostly from the relaxation process, while the number of phonons emitted during non-radiative recombination is negligible.

2. Samples and experimental techniques

The samples were grown on (0001) sapphire substrates by atmospheric pressure metal–organic chemical–vapour deposition (MOCVD). The growth details may be found in [4]. The MQW structures consisted $10 \times (In_{0.13}Ga_{0.87}N)$ QWs separated by 7.5 nm GaN barriers. Three MQW samples were studied having different thicknesses of QWs: 1.25, 2.5 and 5 nm. The backsides of the substrates were polished and superconducting bolometers (40×40 μm active area) were evaporated to detect the phonons. After polishing, the thicknesses of the substrates were between 0.31 and 0.37 mm, depending on the sample.

The samples were mounted in an optical access helium bath cryostat and maintained at constant temperature on the superconducting transition of the aluminium bolometers, $T_0 \approx 2$ K. The excitation source was a frequency-tripled, $\lambda = 355$ nm, Q-switched Nd–YAG laser,

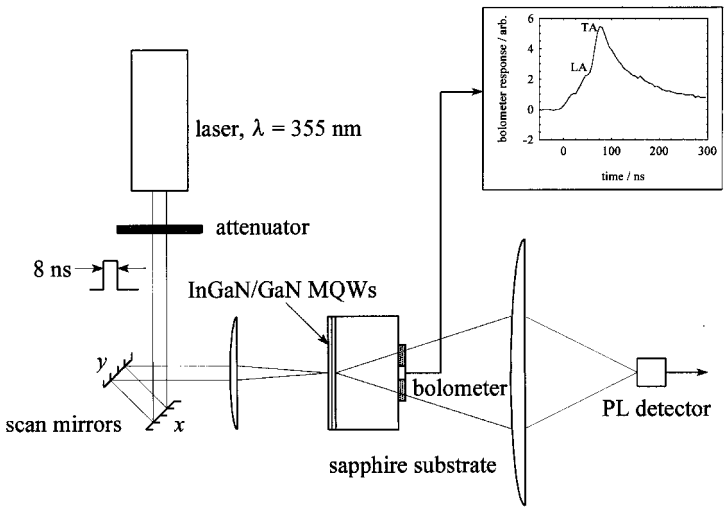

Figure 2. Experimental setup and a typical bolometer signal.

providing 8 ns duration pulses with a maximum energy of $\sim$1 μJ. The laser beam was focussed on a spot of diameter 50 μm on the surface of the sample with the grown MQW structure. Non-equilibrium phonons emitted as the result of hot carrier (exciton) relaxation and non-radiative recombination in the MQW structure traversed the sapphire substrate and fell on the superconducting bolometer warming it slightly. The transient change in resistance of the constant current biased bolometer led to a voltage pulse which was amplified and detected using a high-speed digitizer and signal averager. The overall time resolution of the detection system was $\sim$10 ns. A pair of computer-controlled galavanometer mirrors were used to position the excitation laser spot on the sample's surface. The spot could be raster (x–y) scanned to produce an image (phonograph) of the phonon emission. Acoustic, LA and TA, phonons with energies $\hbar\omega < 10$ meV propagate ballistically in thin (<0.4 mm) sapphire substrates[3]. The typical bolometer response for these ballistic phonons, figure 2(inset), shows a sharp rising edge at the time equal to the time of flight between excitation point and the bolometer corresponding to the phonon group velocity v in sapphire ($v_{\mathrm{LA}} = 11 \times 10^3$ m s^{-1} and $v_{\mathrm{TA}} = 6 \times 10^3$ m s^{-1} for LA and TA phonons respectively).

As well as detecting the emitted phonons, the PL was also measured using a single-grating monochromator and a Si avalanche photodiode detector operating in Geiger mode. The low-temperature ($T_0 = 2$ K) PL spectra are identical to the spectra studied in detail in earlier work [4, 5]. The PL spectrum of each sample consists of a relatively narrow (45 meV width) spectral line peaked at the exciton energy E_{PL} which decreases as the MQW width increases. The measured values of E_{PL} are presented in table 1.

Phonon transport in the substrate is strongly influenced by acoustic phonon focussing. Owing to the elastic anisotropy of the crystal, the phonon group velocity vector is not in general parallel to the phonon wavevector $\boldsymbol{q}$ [12]. This results in an enhancement of the phonon flux along certain crystallographic directions where the curvature of the constant energy surface in k-space (slowness surface) is zero. To illustrate the imaging technique, we present in this section the phonon signals and a phonon image for the case of the blank sapphire substrate

[3] In highly pure crystals that are free of structural defects, the main source of phonon scattering is Rayleigh-type scattering from isotopic mass defects. In sapphire (Al_2O_3), this is mostly due to a 0.2% natural abundance of ^{18}O. Using the method of Klemens [11] we estimate that the phonon mean-free path is approximately equal to the thickness of the substrate at a frequency of 6 THz for TA phonons and 11 THz for LA phonons.

Table 1. MQW parameters

				$q_\parallel$ (10^7 cm^{-1}) for $E_k = 30$ meV		
w (nm)	E_{PL} (eV)	ΔE (eV)	$q_\perp$ (10^7 cm^{-1})	Electrons ($m = 0.2m_0$)	Holes ($m = 0.8m_0$)	Excitons ($m = m_0$)
1.25	3.25	0.27	2.51			
2.5	3.18	0.34	1.26	0.88	1.67	1.87
5.0	3.01	0.51	0.63			

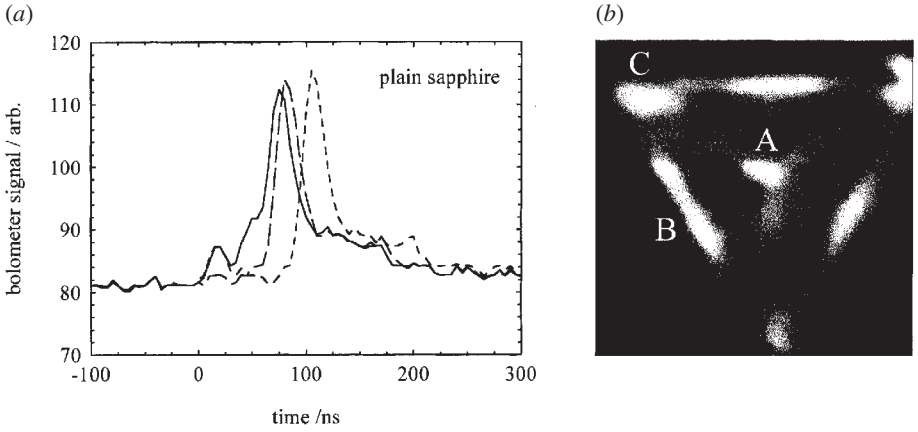

Figure 3. Phonon signals (*a*) and TA phonon image (*b*) measured in a blank sapphire substrate. Phonons are generated in a metal film on the sapphire surface. The phonon signals (*a*) are measured at points A (solid curve), B (dashed curve) and C (dotted curve).

(without the grown InGaN/GaN/GaN structure) which we used as a control sample. In this case, the non-equilibrium phonons were generated by optical excitation of a 100 nm thick metal film evaporated on the sapphire surface opposite the bolometer. Figure 3(*a*) shows the time evolution of the detected signals measured for different positions of the laser spot relative to the bolometer which determined the angle of phonon propagation. The main peak corresponds to acoustic TA phonons. Figure 3(*b*) shows an image of the TA phonon amplitude for a scan area of 1×1 mm^2 with the bolometer at the centre. The light areas of figure 3(*b*) correspond to a larger TA amplitude. It is clearly seen that the phonon signal is mostly concentrated inside a triangle shape, and there are seven bright spots where the intensity of phonon signal is at a maximum: the centre (A) which corresponds to the excitation point opposite the bolometer; three sides (B) and three corners (C) of the triangle (see labels in figure 3(*b*)). More details of the phonon images in sapphire may be found in the earlier work of Every *et al* [13]. The signals in figure 3(*a*) correspond to the three different points (A, B and C) and it is clearly seen that the amplitudes of the TA phonon signals have almost the same value at each point.

In the experiments with InGaN/GaN MQWs we compared the measured signals and phonon images with the reference signals and image shown in figure 3 where the phonons are emitted in the metal film and the angular distribution of phonon wavevectors is believed to be isotropic.

The superconducting bolometer is sensitive not only to emitted phonons, but also to photons, that is, PL from the InGaN/GaN MQW. In order to extract the 'pure' phonon signal, we measured the PL pulses separately using a fast blue/ultraviolet optimized photodiode and subtracted these from the bolometer traces. The PL and bolometer measurements were carried

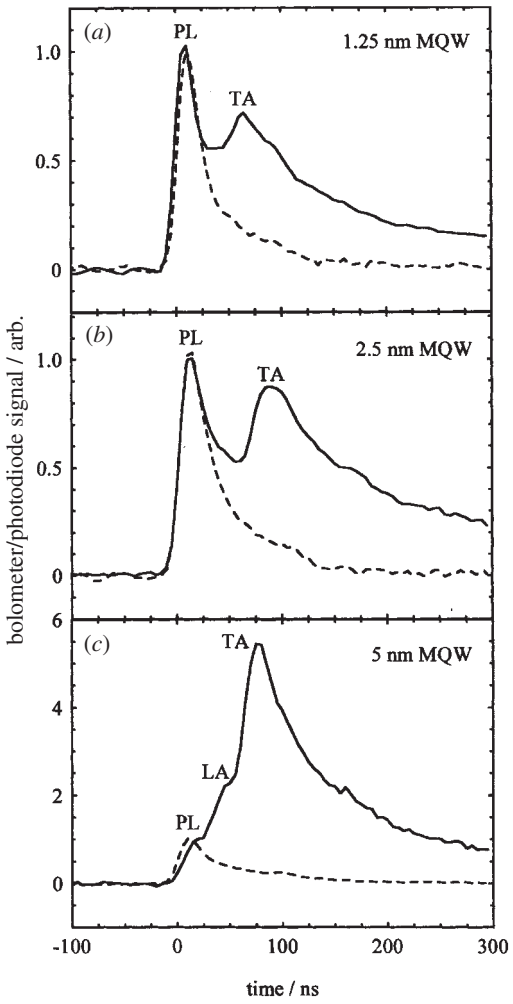

Figure 4. Bolometer (solid curves) and PL (dashed lines) signals measured in the three InGaN/GaN MQWs at $P = 20$ kW cm^{-2} incident at point A opposite to the bolometer. The pulse at $t = 0$ in the bolometer signals corresponds to the optical response of the bolometer.

out in identical geometries and settings for different samples which allows us to analyse the relative intensity of photon and phonon fluxes in different MQW samples and thus get information about the PL quantum efficiency.

3. Experimental results and discussion

3.1. PL quantum efficiency in MQWs

Figure 4 shows the detected bolometer (solid curves) and photodiode (dotted curves) signals in the samples with different MQW widths. The signals are normalized to unity for the PL amplitude in each sample. It is seen that the relative intensity of the phonon component of the signal increases as the MQW width increases. The phonon contribution is at a maximum in the wide 5 nm MQW where the amplitude of the TA signal is about five times bigger

than the amplitude of the PL pulse. In sharp contrast, the TA amplitude is smaller than the PL signal in the narrow 1.25 nm MQW. Separate measurements of the PL signal show that the PL pulses have the same amplitude in the 1.25 and 2.5 nm MQWs while, in the 5 nm MQW, the PL amplitude is about 60% of that in the other two samples. The relative values of the low-temperature PL intensities are in good agreement with the earlier studies of similar MQWs, where it was shown that the 2.5 nm MQW has a higher quantum efficiency than the wider 5 nm MQW [5]. The temporal dependence of the PL signals measured by the photodiode (dashed curves in figure 4) is almost the same for all three MQW samples and is determined by the overall temporal resolution of the optical and electronic detection systems. However, in agreement with earlier studies [7], we found that the PL decay for the 5 nm MQW is slightly longer than for other, narrower, MQW samples.

We explain the results in figure 4 in terms of the different PL quantum efficiencies for the different MQWs. The total amount of energy, E_{ph}, emitted as phonons by the hot carriers and excitons may be written

$$E_{\mathrm{ph}} = \Delta E + (1 - \eta) E_{\mathrm{PL}} \tag{1}$$

where $\Delta E = E_0 - E_{\mathrm{PL}}$ is the excess energy released during relaxation of the hot carriers and excitons. The second term in (1), which includes the PL quantum efficiency η, describes the energy released as a result of non-radiative recombination. If we assume that $\eta = 1$ in the 1.25 and 2.5 nm MQW samples and, correspondingly, $\eta = 0.6$ in the 5 nm MQW (based on the relative sizes of the PL pulse), then from (1) using the values for ΔE (see table 1) we can calculate the ratios of the total phonon emitted energies as $1/1.3/6.3$ for 1.25, 2.5 and 5 nm MQWs, respectively. Comparing the detected bolometer and photodiode signals (figure 4) we get the corresponding phonon amplitude ratios equal to $1/1.4/5.6$ which is in good agreement with the calculated values. The small difference in experimental and calculated ratios may be due to different angular and temporal dependencies of the detected phonon signals for different MQW samples (see the next section). It should be noted that, in our experiments, the excitation energy $E_0 = 3.52$ eV $\approx E_{\mathrm{GaN}}$ at $T = 2$ K (E_{GaN} is the band gap in the GaN barriers) and so the relaxation path is mainly within the two-dimensional MQWs while the amount of phonons emitted from the bulk GaN barriers can be neglected.

The results of the analysis based on (1) and comparison with the experimental data leads us to conclude that the 1.25 and 2.5 nm MQWs have a low-temperature PL quantum efficiency that is close to unity. The same statement was claimed in previous work on similar samples [4,5]. Hence in the 1.25 and 2.5 nm MQWs, the emission of phonons is mainly from the relaxation of hot carriers and excitons. Non-radiative recombination processes compete with radiative processes and lead to a reduction of the PL quantum efficiency when the non-radiative recombination time becomes comparable to, or shorter than, the radiative lifetime (typically $\sim$1 ns in III–V semiconductors). This is probably the case for the 5 nm MQW sample, in which we measure a quantum efficiency of 0.6. Further work is required to obtain information about the microscopic details of the non-radiative processes. However, at this time, we can say that our phonon data is not inconsistent with the explanation given in [7] for the longer PL decay time in wider MQW samples. That is, owing to the very strong spontaneous PE polarization fields at the GaN/InGaN interfaces, the bands are tilted in the QWs and this band-tilting effect is larger in the wider wells. The electron and hole wavefunctions are therefore confined near the edges of the wells and the reduced wavefunction overlap leads to an increase in the radiative lifetime (quantum confined Stark effect). Non-radiative recombination, possibly as a result of exciton tunnelling between tail states extending into the InGaN gap from the conduction and valence band edges, may then make a significant contribution.

3.2. Angular distribution of phonon emission in the MQWs

Figure 5 shows the 'pure' phonon signals obtained by subtracting the appropriate PL signals from the measured bolometer traces. The data are presented for two MQW samples: 1.25 nm in figures 5(*a*)–(*c*), and 2.5 nm in figure 5(*d*), and different peak optical excitation densities P. Each set shows the temporal evolution for phonons emitted at the three excitation points labelled in figure 3(*b*): A (solid curves); B (dashed curves) and C (dotted curves). Full images of the TA phonon signal amplitude are shown in figure 6.

It can be seen that in the 1.25 nm MQW at low $P(\lesssim 3$ kW cm$^{-2})$, the phonon signal is the biggest for the excitation point A which is located directly opposite the bolometer (figure 5(*a*)). Correspondingly, the image (figure 6(*a*)) shows a bright spot in the centre while the side features of the phonon focussing triangle are weak. Such behaviour is very different from the case of isotropic emission of phonons in a metal film (figure 3) where the phonon signals have similar amplitudes at points A, B and C. Thus the emission of phonons in the 1.25 nm MQW is strongly anisotropic, the phonons being emitted mostly perpendicular to the plane of the MQW. This anisotropy becomes much less pronounced for elevated $P = 20$ kW cm^{-2} (figure 5(*b*)) and for higher $P \gtrsim 34$ kW cm^{-2} the angular distribution of emitted phonons becomes almost the same as in the case of the metal film source on sapphire (compare figure 5(*c*) and the phonon image in figure 6(*b*) with figure 3).

An example of the phonon signals and image measured in the 2.5 nm MQW for $P = 3$ kW cm^{-2} is shown in figures 5(*d*) and 6(*c*), respectively. The results for this MQW sample do not differ significantly from the isotropic case of the metal film source (figure 3). We may therefore conclude that phonon emission in the 2.5 nm MQW has an isotropic angular distribution for all P. The emission of phonons in the 5 nm MQW was also found to be isotropic. To check that the angular dependence was not affected in any way by phonon transport across the GaN/sapphire interface, we also measured the phonon signals and images for pure bulk GaN layers. The emission of phonons in these bulk samples is isotropic and, as expected, the results were also similar to the case of the metal film source (figure 3).

Comparing figures 3 and 5 we see that all phonon signals produced by optical excitation of MQWs have a much longer decay tail than signals from the metal film. It is well known that such a long tail corresponds to high-energy acoustic phonons which are strongly scattered on the way from the excitation point to the bolometer [14]. The long tail measured in the MQW samples shows that optical excitation of the MQWs tends to generate a high proportion of high-energy phonons.

We begin the discussion of the experimental results with a description of relaxation paths for hot carriers and excitons in the MQWs. The excess energy in all MQW samples is higher than the energy of the GaN LO phonon ($\hbar\omega_{\mathrm{LO}} = 92$ meV). The emission of LO phonons is governed by the very efficient Fröhlich interaction and the corresponding carrier (exciton)–phonon transition rate is much higher than for acoustic phonons [9]. Therefore, several LO phonons should be emitted as a result of carrier and exciton relaxation. To determine exactly the proportion of ΔE that is lost by emission of LO phonons requires knowledge of the carrier relaxation dynamics in the InGaN/GaN system. Specifically, whether electrons and holes relax their excess energy as separate particles or as the composite particle (exciton). Currently this is not known for GaN-based structures. Analysing the different possible paths for relaxation at low-excitation densities, we find that not more than 2 (for the 1.25 nm MQW) or 3 (for the 2.5 nm MQW) LO phonons may be emitted during the relaxation process. The remainder of the excess energy (<92 meV) is emitted mainly as acoustic phonons.

The observed anisotropy for the phonon emission in the 1.25 nm at low power (figures 5(*a*), (*b*) and 6(*a*)) is in agreement with the theoretical considerations for acoustic

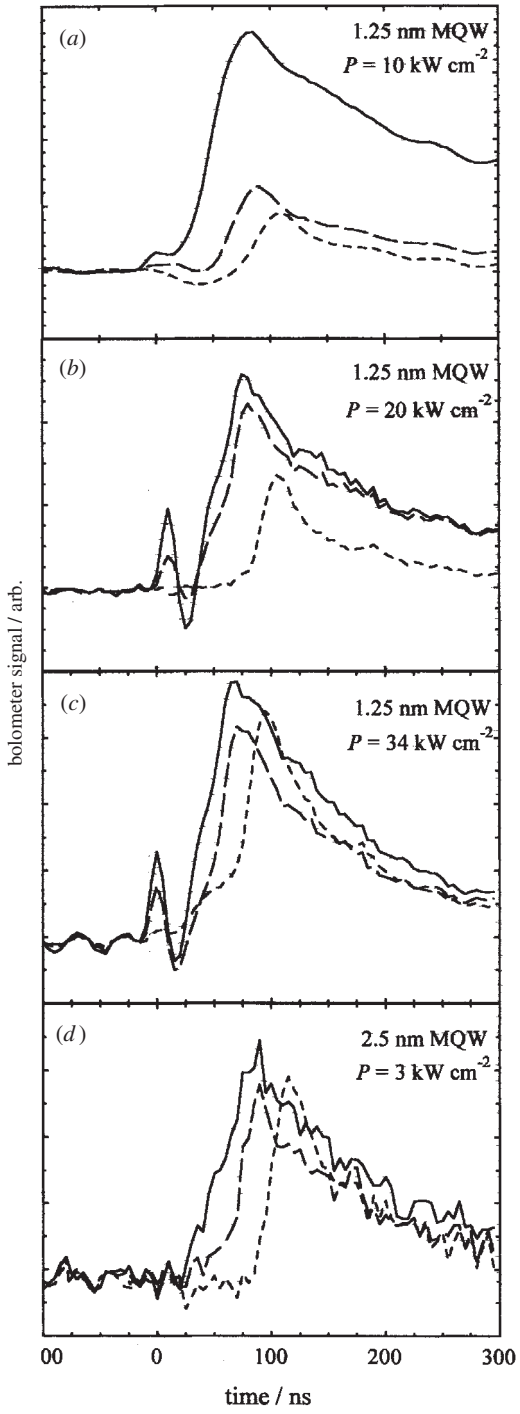

Figure 5. Phonon signals obtained in 1.25 nm (*a*)–(*c*) and 2.5 nm (*d*) InGaN/GaN MQWs at points A (solid curves), B (dashed curves) and C (dotted curves). The PL contribution is subtracted from the bolometer signals to give these traces. The optical pickup at $t = 0$ corresponds to the residual PL pulse.

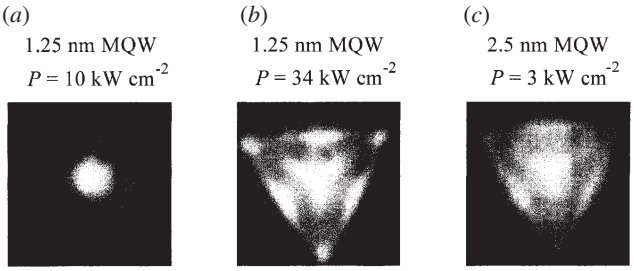

Figure 6. TA phonon images obtained in 1.25 nm (*a*), (*b*) and 2.5 nm (*c*) InGaN/GaN MQWs for low (*a*), (*c*) and high (*b*) excitation densities P.

phonon emission from narrow QWs [15]. The maximum values of the wavevector projections parallel, $q_{\shortparallel}$, and perpendicular, $q_{\perp}$, to the plane of MQW for the acoustic phonons which are active in the interaction with hot quasiparticles are determined by momentum conservation. The in-plane momentum conservation condition for carrier (exciton)–phonon interaction gives

$$q_{\shortparallel} \approx 2k = \frac{2\sqrt{2mE_k}}{\hbar} \tag{2}$$

where k, m and E_k are the quasiparticle wavevector, effective mass and kinetic energy, respectively. The maximum perpendicular component of $\boldsymbol{q}$ is governed by the overlap integral in the matrix element and it is easy to show that

$$q_{\perp} \sim \pi w^{-1} \tag{3}$$

where w is the MQW width. The ratio between $q_{\parallel}$ and $q_{\perp}$ depends on m and E_k. As an example, table 1 shows the calculated values for $q_{\parallel}$ and $q_{\perp}$ at $E_k = 30$ meV in different MQWs for different quasiparticles. It is seen that in the 1.25 nm MQW, $q_{\perp} > q_{\parallel}$ even for the heaviest quasiparticle which is an exciton. Therefore, acoustic phonons will be emitted mostly perpendicular to the MQW plane. The total phonon wavevector for phonons emitted by exciton relaxation in the 1.25 nm MQW is $q \approx 3.1 \times 10^7$ cm^{-1}. This value corresponds to the TA phonon energy $\hbar\omega_{\mathrm{TA}} = \hbar s_{\mathrm{TA}} q = 5.2$ meV ($s_{\mathrm{TA}} = 2.7 \times 10^5$ cm s^{-1}—the TA sound velocity in GaN). Phonons with these energies can propagate ballistically in a sapphire substrate [11]. Thus the above estimates show that the experimentally observed anisotropy in the 1.25 nm MQW is due to the specific features of the electron (exciton)–phonon interaction in two-dimensional systems.

The calculated values of $q_{\parallel}$ and $q_{\perp}$ (see table 1) show that in the 2.5 and 5 nm MQWs the anisotropy of acoustic phonon emission will be much less pronounced than in the 1.25 nm MQW. Moreover, in the wider MQWs the proportion of ΔE emitted as acoustic phonons is smaller. Non-radiative recombination also provides a channel for isotropic phonon emission in the 5 nm MQW. All these arguments account for why the phonon emission in the wider, 2.5 and 5 nm MQWs, is observed to be isotropic.

Emission of LO phonons makes the dominant contribution to the total emitted energy in all the MQW samples. Optical phonons have a small group velocity and do not propagate to the bolometer, but decay to high-energy acoustic phonons ($\hbar\omega_{\mathrm{TA}} \gtrsim 20$ meV) on a picosecond timescale [16]. Such acoustic phonons do not propagate ballistically in sapphire and do not have a sufficiently long lifetime to reach the bolometer before down-converting. The detailed analysis of the kinetics of these phonons is complicated, but it is clear that the LO decay products will reach the bolometer with a delay causing the long tails which are observed experimentally (figure 5).

It is interesting to note that the angular distribution of emitted phonons in the 1.25 nm MQW depends on the excitation power P. The anisotropy of phonon emission smoothly disappears with the increase of P (refer to figures 5(b), (c) and the image in 6(b)). We account for this by the increased role of many-body interactions at high-quasiparticle densities. We estimate the sheet density of electron–hole pairs $n_s \sim 5 \times 10^{12}$ cm^{-2} for $P = 30$ kW cm^{-2}. At such high n_s values, the carriers and excitons form a thermalized distribution with $T \gg T_0$. The average excess power per pair is $\sim$1 nW and using the standard expression for the energy loss by hot two-dimensional carriers [15] we estimate that $T \approx 140$ K. At such high T values, mostly LO phonons are emitted [9]. Therefore, at high-excitation power levels, most of the acoustic phonons detected by the bolometer are the products of LO phonon decay and the angular distribution of these is expected to be isotropic. Only at low P, when carrier–carrier (carrier–exciton and exciton–exciton) collisions may be neglected, would we expect to observe the anisotropic emission of acoustic phonons from the 1.25 nm MQW.

4. Conclusions

We have measured the angular and excitation power dependencies of phonon emission by optically excited InGaN/GaN MQWs with three different well widths. The results show that for the narrow 1.25 nm MQW and low-excitation power $P < 20$ kW cm^2, the emission of acoustic phonons is anisotropic and phonons are emitted mostly perpendicular to the MQW plane. This is in agreement with estimations based on the theory of electron–phonon interaction in two-dimensional semiconductor nanostructures. In wider MQWs the phonon emission is isotropic which we have explained by considering the relaxation and non-radiative recombination processes.

We also show that for the narrow, 1.25 and 2.5 nm, MQWs the PL quantum efficiency is close to unity and phonon emission is mainly due to hot carrier and exciton relaxation. In the wider 5 nm MQW, the PL quantum efficiency is reduced to about 0.6 and non-radiative recombination processes also contribute to phonon emission.

Our results show that these MQWs provide model systems for studying the fundamental properties of relaxation by optically excited quasiparticles in two-dimensional GaN nanostructures using phonon-emission experiments.

Acknowledgments

The authors acknowledge financial support for this work from EPSRC of the UK, under grants nos GR/M04365 and GR/M82295. They would also like to thank Professor C T Foxon for helpful discussions.

References

[1] Nakamura S, Senoh M, Iwasa N and Nagahama S 1995 *Japan. J. Appl. Phys.* **34** L797
[2] Nakamura S, Senoh M, Nagahama S, Iwasa N, Yamada T, Matsushita T, Kiyoku H and Sugimoto Y 1996 *Japan. J. Appl. Phys.* **35** L217
[3] Nakamura S and Fasol G 1997 *The Blue Laser Diode* (Berlin: Springer)
[4] Wang T, Nakagawa D, Wang J, Sugahara T and Sakai S 1998 *Appl. Phys. Lett.* **73** 3571
[5] Wang T, Nakagawa D, Wang J, Sugahara T and Sakai S 1999 *Appl. Phys. Lett.* **74** 3128
[6] Narukawa Y, Kawakami Y, Shizuo Fujita, Shigeo Fujita and Nakamura S 1997 *Phys. Rev.* B **55** R1938
[7] Davidson J A, Dawson P, Wang T, Sugahara T, Orton J W and Sakai S 2000 *Semicond. Sci. Technol.* **15** 497
[8] Martin R W, Middleton P G, O'Donnell K P and Van der Stricht W 1999 *Appl. Phys. Lett.* **74** 263
[9] Stanton N M, Kent A J, Akimov A V, Hawker P, Cheng T S and Foxon C T 2001 *J. Appl. Phys.* **89** 973

[10] Jasiukiewicz Cz, Lehmann D, Kent A J, Cross A J and Hawker P 1999 *Physica* B **263–4** 183
[11] Seitz F and Turnbull D (ed) 1958 *Solid State Physics* (New York: Academic)
[12] Wolfe J P 1998 *Imaging Phonons* (Cambridge: Cambridge University Press)
[13] Every A G, Koos G L and Wolfe J P 1984 *Phys. Rev.* B **29** 2190
[14] von Gutfeld R J 1969 *Physical Acoustics* vol 5 (New York: Academic) p 233
[15] Kent A J 1988 *Hot Electrons in Semiconductors: Physics and Devices* ed N Balkan (Oxford: Clarendon) p 81
[16] Ridley B K 1996 *J. Phys.: Condens. Matter* **8** L511